Effect of Ligand and Solvent Structure on Size-Selective Nanoparticle Dispersibility and Fractionation in Gas-Expanded Liquid (GXL) Systems

ARTICLE *in* THE JOURNAL OF PHYSICAL CHEMISTRY C · JUNE 2013

Impact Factor: 4.77 · DOI: 10.1021/jp403670w

THE JOURNAL OF PHYSICAL CHEMISTRY C

Article

pubs.acs.org/JPCC

Effect of Ligand and Solvent Structure on Size-Selective Nanoparticle Dispersibility and Fractionation in Gas-Expanded Liquid (GXL) Systems

Pranav S. Vengsarkar and Christopher B. Roberts*

Department of Chemical Engineering, Auburn University, 212 Ross Hall, Auburn, Alabama 36849-5127, United States

Supporting Information

ABSTRACT: Nanoparticles have highly size-dependent properties which need to be harnessed for their appropriate use in various applications. One method that has been used to obtain monodisperse nanoparticles involves the initial synthesis of a relatively polydisperse nanoparticle dispersion using conventional methods, followed by the size-selective separation of these nanoparticles using a variety of different processing techniques. Through prior investigations in our group, we have demonstrated that application scale quantities of ligand-stabilized metal nanoparticles can be precisely separated based upon their size via a sequence of pressure-induced precipitations from gas-expanded liquid (GXL) mixtures (typically a mixture of an organic solvent and compressed CO_2 gas). However, this solvent-based process requires relatively high applied pressures of CO_2 (e.g., ~41.4 bar with *n*-hexane as the solvent and dodecanethiol as the ligand) to effectively precipitate these nanoparticles from the solvent + CO_2 mixture. In this paper, through methodic selection of solvents and ligands of different steric structures, we have aimed to manipulate the nature of the solvent−ligand interaction so as to precipitate and size-selectively fractionate gold nanoparticles at lower pressures in these GXL systems. Constitutional isomers of *n*-hexane were chosen as the solvents in this study while dodecanethiol and its isomer, *tert*-dodecanethiol, were used as the stabilizing ligands. Ultimately, it was deduced that using a combination of branched solvent (2,2-dimethylbutane) and branched ligand (*tert*-dodecanethiol) caused the nanoparticles to precipitate from solution at only 6.9 bar. This almost 6-fold reduction in pressure can be attributed to the reduced solvent−ligand interactions in the system relative to straight-chain solvent and straight-chain ligand system. The impact that this altered solvent−ligand interaction has on effectiveness of the GXL size-selective fractionation process is also detailed in this paper. Hence, this study illustrates that one can tune the process parameters critical to the GXL size-selective fractionation process by simply changing the physical interactions between the nanoparticle ligand and the solvent.

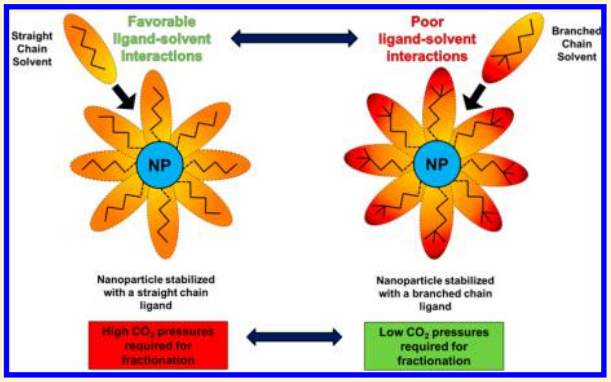

INTRODUCTION

Nanotechnology is an important topic in modern research due to its multidisciplinary applicability and future potential in many applications. Nanoparticles of metals (e.g., gold) and metal oxides (e.g., iron oxide) are major areas of research in this field of study due to their breadth of application in disciplines such as biomedicine,[1−4] surface technology,[5,6] and catalysis.[7−9] For example, gold nanoparticles can be useful as drug delivery agents and in hydrogenation/redox catalysis[8,10] while iron oxide nanoparticles can be used in various applications like Fischer−Tropsch catalysis[11,12] and as contrast agents for MRI.[13−15] Materials with dimensions at these length scales exhibit very unique electrical, optical, magnetic, mechanical, and catalytic properties which deviate from the properties of their bulk constituent material.[16] This nonconformity between the macroscopic properties and nanoscale properties is due to quantum effects that dominate over other effects at these small dimensions[17] as well as the high surface area to volume ratio that is present at this scale. These unique size-dependent properties present the need to develop synthesis and processing procedures which deliver monodisperse nanoparticles. In particular, efficient postsynthesis processing techniques for the effective size-based separation of nanoparticles from polydisperse samples are of paramount importance. There are currently several techniques available to effectively generate monodisperse nanoparticles;[18−24] however, many of these require the use of large amounts of solvents, high temperatures, expensive reagents, and also the use of certain stabilizing ligands that limit surface access/functionality. With regard to postprocessing techniques, the methods currently available include magnetic separation,[25,26] size-exclusion chromatography,[27−31] centrifugation,[29,32] electrophoresis,[33,34] membrane separation,[35,36] and solvent/antisolvent precipitation. However, these techniques are constrained by certain drawbacks,

Received: April 14, 2013
Revised: June 11, 2013
Published: June 13, 2013

including limited size-dependent applicability,[37,38] large amounts of solvents required, low throughputs, and expensive equipment.[39]

One of the methods that was developed to overcome some of the limitations associated with size-selective nanoparticle postsynthesis processing includes the use of gas-expanded liquid (GXL) systems[39−41] in a modified solvent−antisolvent process. This process is referred to as the GXL size-selective fractionation process.[39] In this method a liquid solvent and a gaseous antisolvent (CO_2) are used to precipitate nanoparticles of progressively smaller size from solution using increasing amounts of applied CO_2 pressure. A GXL is a mixed solvent composed of a compressible gas like CO_2 or ethane dissolved in an organic solvent.[42] This gives it pressure tunable properties due to the organic liquid solvent expanding upon gas dissolution. Several properties of the gas-expanded mixture such as viscosity, diffusivity, and solubility are affected by this pressure-tunable solvent expansion. An advantage of this GXL size-selective fractionation process is the fact that the antisolvent (CO_2) can be separated from the liquid simply by depressurization and thereby recovered and reused. CO_2 is typically chosen as the antisolvent for this process because of several advantages that it offers. CO_2 is relatively inert, readily available, is highly soluble in organic solvents, and is a known antisolvent for aliphatic ligands that are used to stabilize nanoparticles during synthesis. Furthermore, it also has no dipole moment and little self-interaction which make it an extremely good antisolvent for these ligands.[41]

Previously, it has been shown that nanoparticle dispersions of different materials like CdSe/ZnS quantum dots and gold nanoparticles can be effectively precipitated using GXLs with CO_2 as the gaseous antisolvent.[39,40,43] In the GXL process, an organic solvent dispersion (e.g., *n*-hexane) of ligand (e.g., dodecanethiol) stabilized metal nanoparticles (e.g., gold) can be precipitated with applied CO_2 pressures below the vapor pressure of CO_2. In this case, CO_2 dissolves into the solvent to a degree proportional to the applied CO_2 pressure and since CO_2 is an antisolvent for the aliphatic ligands the mixture's solvent strength is diminished to an extent such that precipitation of the nanoparticles can be achieved. When the organic solvent nanoparticle dispersion is pressurized with CO_2 to the extent that only a fraction of the nanoparticles precipitate, the other nanoparticle fraction has to be separated from the system such that an effective fractionation can be achieved. It is noted that the largest nanoparticles will precipitate first upon worsening solvent conditions (i.e., with increasing applied CO_2 pressure) due to larger van der Waals forces.[39,40] This GXL size-selective fractionation process has been successfully applied in previous studies to a number of polydisperse nanoparticle systems.[39,44,45]

While this process gives relatively monodisperse particles, it is still necessary to subject the system to significant applied pressures of CO_2. Usually, applied CO_2 pressures of around 35 bar are required to begin the precipitation of gold nanoparticles coated with dodecanethiol dispersed in *n*-hexane.[41] In this paper, the pressure at which the nanoparticles start to precipitate from the solvent dispersion will be referred to as the pressure of incipient precipitation (P_i). It has been shown in previous studies[44,46] that reduction of P_i values is feasible by modifying solvent−ligand interactions, and this was obtained using short-chain solvents (e.g., pentane), short-chain ligands (e.g., hexanethiol), and cosolvents (e.g., acetone). However, insignificant P_i reduction was obtained using short-chain solvents, and only moderate reduction in P_i values was obtained using short-chain ligands.[46] Also, nonspherical particles were observed due to the use of these short-chain ligands which can be explained by the possible insufficient steric stabilization provided by these ligands after the growth phase during the synthesis procedure. By using cosolvents combined with short-chain ligands, the P_i values were tuned successfully from 35 to 5 bar to still obtain monodisperse nanoparticles.[44] While the use of cosolvents and shorter ligands is advantageous to reduce pressures, it is also difficult to control and predict sizes obtained due to presence of the cosolvent, which adds an extra variable to the entire system. Also, since short-chain ligands were used again with the cosolvents, the problem with misshapen particles was observed again with these systems.[44]

The main aim of this paper is to check the feasibility of reducing the operating pressures in the GXL fractionation process with the goal for making this process more economically viable, through the modification of the ligand and solvent steric structures and manipulation of the solvent−ligand interactions. Moreover, this study should be critical in furthering our understanding of the changes in solvent−ligand interactions due to change in ligand and solvent structure and how these interactions affect nanoparticle dispersibility in gas-expanded liquids.

EXPERIMENTAL SECTION

Materials. Gold(III) chloride trihydrate ($HAuCl_4{\cdot}3H_2O$, 99.9%), sodium borohydride ($NaBH_4$, >98.0%), tetraoctylammonium bromide (TOABr, $[CH_3(CH_2)_7]_4NBr$, 98%), 1-dodecanethiol ($CH_3(CH_2)_{11}SH$, 98%), and *tert*-dodecanethiol (mixture of isomers) ($CH_3(CH_2)_8C(CH_3)_2SH$, 98.5%) were obtained from Aldrich. *n*-Hexane (HPLC grade, 95%), 2-methylpentane (99+%), 3-methylpentane (99+%), 2,2-dimethylbutane (99%) and 2,3-dimethylbutane (99+%) were obtained from Alfa-Aesar. Ethanol (94.0−96.0%) was obtained from Mallinckrodt Chemicals. Toluene (HPLC grade, 99.9%) and (deionized ultrafiltered) DIUF water were obtained from Fisher. Carbon dioxide (SFC/SFE grade) was obtained from Airgas. All chemicals were used as received without further purification.

Gold Nanoparticle Synthesis. For the synthesis of dodecanethiol-capped gold nanoparticles dispersed in an organic solvent, the two-phase arrested precipitation method developed by Brust et al.[47,48] and then modified by Sigman et al.[49] was used. A solution of gold salt was initially prepared by dissolving 0.36 g of $HAuCl_4{\cdot}3H_2O$ to 36 mL of water. Also, a solution TOABr was prepared by completely dissolving 2.7 g of TOABr in 24.5 mL of toluene. The gold−salt solution was then slowly added to the TOABr solution on a magnetic stir plate, and a color change was observed. This mixture was then vigorously stirred for an hour, and then the aqueous phase was removed using a pipet. A solution of $NaBH_4$ (0.5 g of $NaBH_4$ in 30 mL of DIUF water) was then slowly added over a period of 1 min to the remaining organic mixture, while still being stirred, in order to induce reduction of the salt. This mixture was allowed to stir, at room temperature, for 8 h, and then the new aqueous layer was removed. Following complete aqueous layer removal, 240 μL of 1-dodecanethiol (or *tert*-dodecanethiol as appropriate) was added to the solution and was stirred for a further 4 h. To purify the sample, 40 mL of ethanol was first added to precipitate the nanoparticles. The solution was then centrifuged (Labnet Hermle Z200A) at 5000 rpm for 5 min, and the supernatant was discarded. This purification process

with ethanol was performed three times in succession to remove any impurities from solution such as excess 1-dodecanethiol. The solution was then dried using nitrogen and then redispersed in the solvent of choice.

Monitoring Nanoparticle Dispersibility Using UV−vis Spectroscopy. The absorption spectra of metallic gold nanoparticles is characterized by a strong broad absorption band at around 520 nm that is absent in the bulk metal spectra.[50,51] This absorption band can be used to determine the dispersibility of gold nanoparticles in solution. The conditions present in an expanding GXL containing gold nanoparticles can also be traced effectively by using this surface plasmon resonance (SPR) band of the gold nanoparticles.[41] This unique absorbance band is credited to the collective oscillation of the conduction electrons in the gold nanoparticles in response to external optical excitation.[52] The presence of this band in the visible region of the spectrum is responsible for the striking colors of dilute colloidal solutions of noble metals like gold and silver.[53] The change in intensity of this band can be used to track the precipitation of the gold nanoparticles from the GXL, where greater intensity of the SPR band corresponds to the dispersibility of more nanoparticles (i.e., greater concentration) in the solvent mixture (i.e., *n*-hexane + CO_2).[39,41,46] These UV−vis measurements are performed through the use of a high-pressure vessel fitted with quartz windows, and the entire apparatus is fitted within a UV−vis spectrophotometer (Cary 3E) in order to obtain *in situ* readings of the absorption spectra as a function of applied CO_2 pressure.[41,46] Specifically, the gold nanoparticle dispersion was added to a 1 cm × 1 cm quartz cuvette, and this cuvette was inserted into the high-pressure vessel in alignment with the quartz windows such that an absorption spectrum of the contents of the cuvette can be collected *in situ*. The vessel is purged of air and then pressurized to a desired pressure using CO_2 from a high-pressure syringe pump (ISCO 260D). This initial pressure was chosen such that a certain fraction (the largest particles) of the nanoparticles would precipitate upon dissolution of CO_2 into the solvent so as to form a solvent + CO_2 mixture. The concentration of CO_2 in this mixture is dependent on the CO_2 pressure applied on the system. For the sake of consistency, the change in applied pressure between successive readings was chosen to be 50 psig (i.e., 3.45 bar). The CO_2 pressure within the system was monitored using a pressure transducer attached to the top of the high-pressure vessel and another that was present inline between the pump and the vessel. The system was then allowed to reach equilibrium as evidenced by a consistent UV−vis spectrum as a function of time at that pressure. The system was then pressurized to a subsequent higher pressure so as to further precipitate more nanoparticles (the next smaller sized set of particles), and the UV−vis spectrum was collected again once equilibrium was obtained. This process was continued until the SPR band had completely diminished in the obtained spectra which meant that all the particles had precipitated from the solution. As an example, the UV−vis spectrum for the dodecanethiol-capped gold nanoparticles dispersed in *n*-hexane system is shown in Figure 1. The change in intensity of the SPR band (specifically, the absorbance at 520 nm) is then plotted as a function of applied CO_2 pressure after correcting the initial value for the volume expansion that occurs in the GXL system. This plot then allows for determination of the pressures required to initiate nanoparticle precipitation and the pressure range over which the precipitation occurs. These particular plots are referred to as "precipitation curves" within the remainder of this paper. A generic representation of a precipitation curve of this type is shown in Figure 2. As an example, the precipitation curve for the system where dodecanethiol-capped gold nanoparticles are dispersed in *n*-hexane is shown in Figure 3.

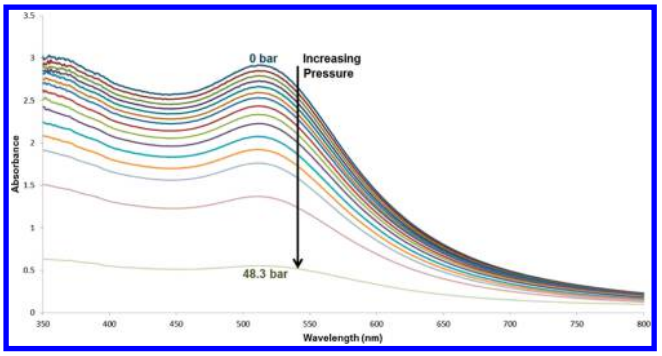

Figure 1. UV−vis spectra for dodecanethiol-coated gold nanoparticles dispersed in *n*-hexane at different applied CO_2 pressures in 3.45 bar intervals (i.e., 50 psig).

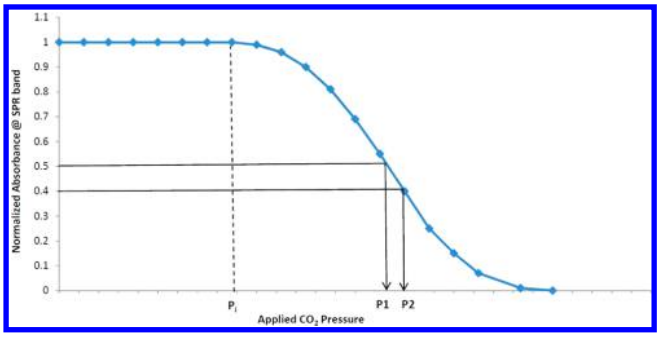

Figure 2. A generic representation of a nanoparticle precipitation curve where P_i corresponds to the "pressure of incipient precipitation" and *P*1 and *P*2 are the pressures employed in the GXL fractionation process, corresponding to the normalized absorbance values of 0.5 and 0.4, respectively.

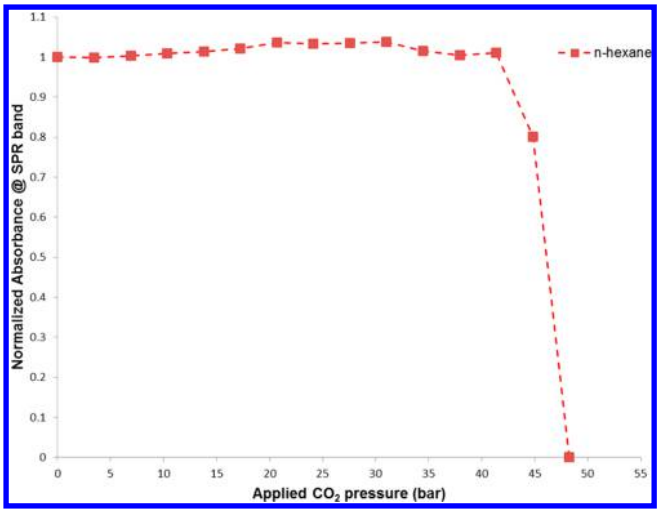

Figure 3. Precipitation curve for dodecanethiol-coated gold nanoparticles dispersed in *n*-hexane obtained by tracking the change in intensity of normalized SPR band using *in situ* UV−vis spectroscopy at different pressures.

Determining the Volume Expansion of Branched Solvents. The decrease in the intensity of the SPR band that occurs upon increasing the degree of CO_2 pressurization is due to two phenomena occurring simultaneously. The first phenomenon is due to the dilution of the dispersion that is caused by the addition of condensed CO_2 into the solvent (so as to create a solvent + CO_2 mixture). The second phenomenon involves the decrease in nanoparticle concentration within the solvent mixture that is caused by the precipitation of the nanoparticles from the solution upon decreasing solvent strength through the addition of CO_2. The dilution effect can be corrected by using volume expansion data from experimental results obtained by visually monitoring the solvent expansion in a graduated Jerguson site gage or by using VLE (vapor−liquid equilibrium) information determined from the Peng−Robinson equation of state (PR-EOS). The correction of intensity of the SPR band was carried out using the Beer−Lambert law assuming a negligible change in the extinction coefficient of the dispersed nanoparticles. For the *n*-hexane + CO_2 system, the experimental expansion data were verified against and found to closely match the volume expansion predicted from the PR-EOS. For the other alkanes, experimental volume expansion data were obtained using the graduated Jerguson site gage, and this data was used in correcting the intensity of the SPR band. This volume expansion data is provided in Supporting Information Figure S1.

Size-Selective Fractionation Process. This work employed a GXL size-selective nanoparticle separation process previously developed at Auburn University in order to obtain monodisperse nanoparticle fractions from a more polydisperse sample as described in detail elsewhere.[39] Specifically, this process allows for monodisperse nanoparticle samples to be separated from an initially polydisperse sample by inducing the controlled precipitation of a fraction of these nanoparticles to occur at a specific location in the apparatus through the application of elevated levels of CO_2 pressure. In short, the apparatus consists of three stainless steel Jerguson site gages (i.e., high pressure vessels J_1, J_2, J_3) which are connected to each other vertically (in series) and are compartmentalized with high pressure valves (V_1, V_2, V_3) and tubing, as illustrated in Figure 4. In addition, each vessel has a glass-tube insert (with a capacity of 20 mL) which is attached to the bottom of the vessel with a liquid tight seal. This allows for easy removal of nanoparticles that will be deposited onto its surface through the course of the following process. A pressure transducer is connected to the top of the first vessel (J_1) to allow for the measurement of the CO_2 pressure.

In a typical experiment, a sample of the liquid nanoparticle dispersion (5 mL) is loaded into the top vessel (J_1), the valve V_1 is closed so as to isolate the solution in J_1, and CO_2 is passed through the entire system (vessels J_1, J_2, and J_3) to purge the system of air and saturate it with hexane vapor. The system is then pressurized to an initial (the lowest) pressure (i.e., P1) which is below the vapor pressure of CO_2 and allowed to equilibrate such that the first fraction of nanoparticles (the largest) is precipitated from the solution onto the walls of the inner glass tube in vessel J_1, leaving the smaller nanoparticles still dispersed in the solution mixture (solvent + CO_2). The valve (V_1) connecting the first and second vessel is slowly opened to allow the remaining dispersed particles to flow into the second vessel (J_2) via gravity. It must be noted that vessels J_2 and J_3 are equipped with side ports that allow for removal of

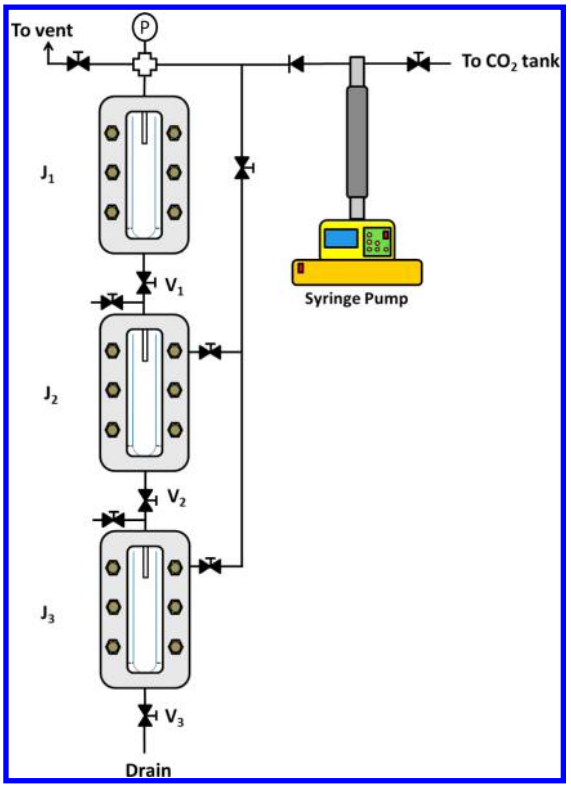

Figure 4. Cascaded vessel apparatus for the size-selective fractionation of nanoparticles using GXLs.

CO_2 gas that must be displaced during the transfer of a liquid dispersion from one vessel to the next at constant pressure (i.e., as a liquid sample is moved from one vessel to the next through the high-pressure valves and tubing, a commensurate volume of gas must be displaced into the former vessel at the same pressure).

After complete transfer of the liquid dispersion to the second vessel (J_2), the system is then pressurized to the second higher pressure (*P*2) which further induces the precipitation of second fraction of the nanoparticles (with sizes smaller than the first fraction). The remaining nanoparticle solution mixture, containing the still dispersed smallest nanoparticles, is then transferred (via V_2) to the last vessel (J_3), and then the system is depressurized slowly. The smallest nanoparticles are obtained as a dispersion by simply draining the solution from the last vessel (via V_3) while the other fractions can be obtained as dispersions by simply isolating and washing each vessel in succession ($J_3 \rightarrow J_2 \rightarrow J_1$) with the solvent being used (thereby redispersing the precipitated nanoparticles in neat solvent).

This entire process is repeated for each of the ligand−solvent combinations in order to examine the effects of solvent structure and ligand structure on nanoparticle precipitation and therefore the effectiveness of this GXL nanoparticle fractionation process in light of each of these changes. Carbon-coated TEM grids of each of the collected nanoparticle fractions were then prepared via drop-casting, and micrographs were acquired on a Zeiss EM 10 transmission electron microscope and sized using the ImageJ software package (more than a 1000 nanoparticles for each sample). The polydispersity index (PDI) is a measure of the broadness of the size distribution which can be used to compare size distributions with dissimilar average diameters. A PDI of 1 indicates that all of the nanoparticles in a collected fraction are of exactly the same size

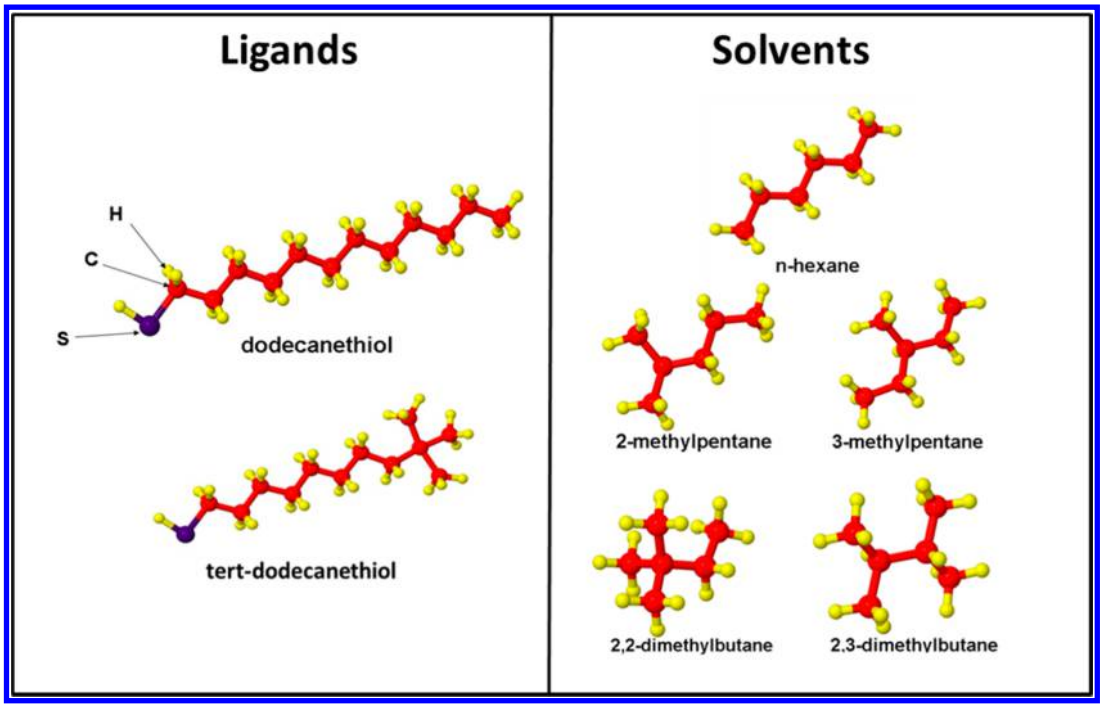

Figure 5. Structures of solvents and ligands used for the experiments carried out in this study.

(therefore, perfectly monodisperse), while larger values of the PDI indicate a broader size distribution of nanoparticles. The PDI is calculated as described elsewhere,[39] where D_i is the size of a specific nanoparticle in a sample of "n" nanoparticles. $\bar{D}_W$ is the diameter-weighted average diameter, and $\bar{D}_N$ is the number-average diameter of the sample. The equations necessary for calculations are as follows:

$$\mathrm{PDI} = \frac{\bar{D}_W}{\bar{D}_N} \quad (1)$$

$$\bar{D}_W = \frac{\sum_i D_i^2}{\sum_i D_i} \quad (2)$$

$$\bar{D}_N = \frac{1}{n}\sum_i D_i \quad (3)$$

RESULTS AND DISCUSSION

The effect that different interactions between solvents and ligands have on nanoparticle precipitation from (and dispersibility in) GXLs can be effectively studied using the techniques described above. The solution of dodecanethiol-capped gold nanoparticles dispersed in *n*-hexane solvent was used as the control for the entire set of experiments presented in this paper since *n*-hexane is a popular solvent in similar nanoparticle dispersion systems and had been researched extensively by our group previously.[39,44] Also, *n*-hexane is an unbranched alkane whose volumetric expansion data can be accurately predicted using the unmodified Peng−Robinson equation of state (PR-EOS).[54−56] Volumetric expansion of *n*-hexane under varying amounts of CO_2 pressure was also measured experimentally in this work in order to verify the applicability of the PR-EOS, and it was determined that the volume expansion as predicted from the PR-EOS very closely matched the experimental data. Dodecanethiol was chosen as the ligand for coating these gold nanoparticles in this control dispersion because it has been shown that dodecanethiol binds more strongly than other straight-chain alkanethiols and the longer thiols result in weakly bound multilayers.[46,57] GXL nanoparticle separation experiments were performed on this control dispersion of dodecanethiol-coated gold nanoparticles in *n*-hexane solvent in order to establish the performance metrics to which the other solvent and ligand systems will be compared later in this paper. The normalized absorbance of the dodecanethiol-coated gold nanoparticles dispersed in *n*-hexane (referred to herein as the dodecanethiol/*n*-hexane system) as a function of the applied CO_2 pressure (i.e., precipitation curve) is presented in Figure 3. From this precipitation curve, it can be observed that the pressure of incipient precipitation (P_i) for the dodecanethiol-coated gold nanoparticles dispersed in *n*-hexane is around 41.4 bar. This relatively high P_i value can be attributed to the straight-chain nature of *n*-hexane which can efficiently stabilize the straight-chain ligands due to its symmetrical structure, thereby requiring higher dissolved CO_2 concentrations in order to destabilize the particles in this solvent. This result is consistent with that reported previously for the precipitation of dodecanethiol stabilized gold nanoparticles from *n*-hexane.[44,55]

Constitutional isomers of *n*-hexane were chosen as the other solvents in this study in order to test the effect of their steric nature on the precipitation and size-selective fractionation of nanoparticles. The use of the constitutional isomers of *n*-hexane allows the steric nature of the solvent to be systematically adjusted in the different experiments in this paper while also allowing the number of carbons in the solvent to be held constant. The same principle of selection was followed for the choice of ligands in this study. The popular and previously studied ligand dodecanethiol[41,55] and its isomer of *tert*-dodecanethiol were used so as to keep the number of carbons in the alkyl chain constant while affording very different steric structures. The structures of the solvents and ligands are shown in Figure 5. It should be noted that *tert*-dodecanethiol is only available commercially as a mixture of its positional isomers,

and a small variation in results due to this variation in steric nature is expected.

1. Straight-Chain Ligand (Dodecanethiol) with Different Solvents (Isomers of *n*-Hexane). The next set of experiments involved varying the structure of the solvent employed, while keeping the ligand (dodecanethiol) structure consistent. These experiments aim to examine the effect that the steric nature of the solvent (i.e., the branched isomers of *n*-hexane) has on gold nanoparticle precipitation, while using particles coated with a straight-chain ligand (dodecanethiol).

1A. Effect of Steric Nature of the Solvent on P_i Values with Dodecanethiol as the Capping Ligand. From the precipitation curves shown in Figure 6, where each of the

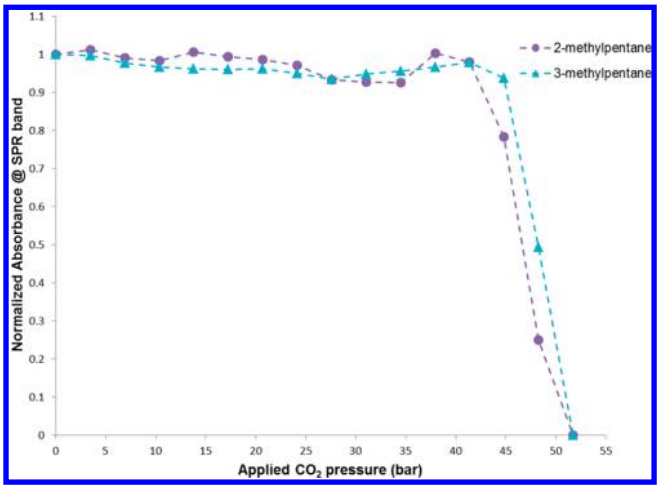

Figure 6. Precipitation curves for dodecanethiol-coated gold nanoparticles dispersed in methylpentanes obtained by tracking the change in intensity of normalized SPR band using *in situ* UV−vis spectroscopy at different pressures.

methylpentanes were used as the solvent, it can be deduced that there is not a significant difference between the precipitation curve for 2-methylpentane/dodecanethiol and 3-methylpentane/dodecanethiol systems. The P_i for both the 2-methylpentane/dodecanethiol and 3-methylpentane/dodecanethiol systems is found to be approximately 41 bar. This similarity in P_i values can be explained from the fact that both these molecules have similar and relatively symmetric structures which should have good interactions with and effectively stabilize the straight-chain ligands. These favorable interactions result in relatively high P_i values being observed. It could be expected that the 3-methylpentane would have a slightly higher P_i value due to its more symmetric nature, but given the 50 psig pressure intervals used during this experimental process, it is not possible to delineate the differences in these precipitation thresholds with any further certainty. As such, the performance of experiments with even smaller pressure intervals would be required to further ascertain the differences in the performance of these slightly different isomers.

However, the precipitation curves that were obtained when using the different dimethylbutanes as solvent (as shown in Figure 7) illustrate more distinct differences in the precipitation curves for 2,2-dimethylbutane/dodecanethiol system and 2,3-dimethylbutane/dodecanethiol systems, with P_i values of approximately 38 and 41 bar, respectively. This difference in P_i values can be attributed to the fact that 2,2-dimethylbutane has a very bulky and branched structure compared to 2,3-

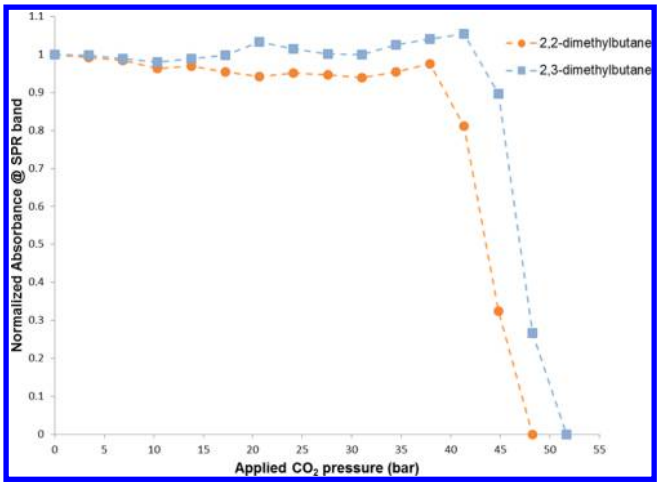

Figure 7. Precipitation curves for dodecanethiol-coated gold nanoparticles dispersed in dimethylbutanes obtained by tracking the change in intensity of normalized SPR band using *in situ* UV−vis spectroscopy at different pressures.

dimethylbutane which has a very symmetric structure. It is expected that the more bulky and/or branched solvents will interact less favorably with the alkyl ligands than simple straight-chain alkane solvents. In this case, the two extra terminal methyl groups that are on the butane chain within the 2,2-dimethylbutane result in increased steric hindrance, thereby resulting in poorer solvent−ligand interactions.

This is reinforced by the fact that highly branched alkanes have negligibly small surface energy compared to straight-chain alkanes.[58,59] The branched-chain solvents are more compact than their straight-chain counterparts, and we would expect them to have a lower surface area. This should result in weaker dispersion forces and hence weaker solvent−ligand interactions in the system.[58,60−62] As such, these weakened interactions should allow us to precipitate nanoparticles from the branched-chain solvent system at lower dissolved CO_2 concentrations, i.e., at a lower overall pressure, than their straight-chain solvent counterparts.

1B. Effect of Steric Nature of the Solvent on GXL Fractionation Process with Dodecanethiol as the Capping Ligand. A series of experiments were performed in order to examine the effectiveness of the GXL fractionation process when utilizing solvents of different steric nature. In order to have a constant frame of reference in all of these experiments, the initial pressure employed in the second stage of the process ($P1$) and the final pressure employed in the second stage of the process ($P2$) were determined from the "precipitation curves" for each respective solvent/ligand system. Specifically, $P1$ was assigned as the pressure that corresponded to the normalized absorbance value of 0.5 in the precipitation curve, and $P2$ was assigned as the pressure that corresponded to the absorbance value of 0.4 in the same precipitation curves (as illustrated in Figure 2). This method of selecting the $P1$ and $P2$ values was based on the premise that particles of approximately the same size and composition should precipitate from each of the solvents within these absorbance values in each of the different sets of experiments.[39,44,45,50,51]

Monodisperse nanoparticle fractions, by definition, means nanoparticles with standard deviation, σ, of diameter less than 5−10%.[63] The nanoparticle fractions in this study, however, do not strictly fit this definition and are only relatively

Table 1. Statistical Summary of Size-Selective Fractionation of Gold Nanoparticles Using CO_2 as GXL

expt no.	ligand	solvent	P_i[a] (bar)	fraction	fraction press. (bar)	ΔP for 2nd fraction (bar)	mean diam (nm)	std dev (nm)	PDI[b]
1	dodecanethiol	*n*-hexane	≈41.4	original		0.35	4.8	1.2	1.06
				1st fraction	0–46.19[c]		5.0	1.1	1.06
				2nd fraction	46.19[c]–46.54[d]		4.6	1.0	1.05
				3rd fraction	46.54[d] and above		3.8	0.8	1.05
2	dodecanethiol	2-methylpentane	≈41.4	original		0.62	4.8	1.0	1.04
				1st fraction	0–46.88[c]		5.4	1.0	1.03
				2nd fraction	46.88[c]–47.50[d]		4.4	1.0	1.05
				3rd fraction	47.50[d] and above		3.0	0.9	1.09
3	dodecanethiol	3-methylpentane	≈41.4	original		0.70	4.6	1.0	1.05
				1st fraction	0–48.60[c]		4.8	0.9	1.03
				2nd fraction	48.60[c]–49.30[d]		3.8	0.8	1.05
				3rd fraction	49.30[d] and above		2.8	1.0	1.13
4	dodecanethiol	2,2-dimethylbutane	≈37.9	original		0.69	4.6	1.0	1.06
				1st fraction	0–43.78[c]		5.2	0.9	1.03
				2nd fraction	43.78[c]–44.47[d]		4.0	0.7	1.03
				3rd fraction	44.47[d] and above		3.0	0.8	1.07
5	dodecanethiol	2,3-dimethylbutane	≈41.4	original		0.69	4.8	1.1	1.06
				1st fraction	0–46.88[c]		4.7	0.8	1.03
				2nd fraction	46.88[c]–47.57[d]		3.9	1.1	1.08
				3rd fraction	47.57[d] and above		3.0	1.0	1.10
6	*tert*-dodecanethiol	*n*-hexane	≈17.2	original		2.07	3.6	1.1	1.10
				1st fraction	0–34.47[c]		4.1	0.7	1.03
				2nd fraction	34.47[c]–36.54[d]		3.6	0.7	1.04
				3rd fraction	36.54[d] and above		3.1	0.8	1.06
7	*tert*-dodecanethiol	2,2-dimethylbutane	≈6.9	original		2.83	3.4	1.0	1.09
				1st fraction	0–26.13[c]		4.4	1.0	1.05
				2nd fraction	26.13[c]–28.96[d]		4.0	0.8	1.04
				3rd fraction	28.96[d] and above		3.4	0.8	1.06

[a]P_i = pressure of incipient precipitation. [b]PDI = polydispersity index. [c]*P*1. [d]*P*2.

monodisperse compared to the original samples. While the selection of *P*1 and *P*2 based on specific absorbance values does allow for particle fractions of similar particle size to be obtained in each of the experiments (i.e., with the different solvents/ligands), it does not necessarily optimize the effectiveness of the fractionation process based on other parameters (such as yield of particles in the different fractions, monodispersity, or the use of constant pressure intervals when collecting each fraction). Nonetheless, it was important in this set of experiments to be able to compare the effectiveness of obtaining particles of similar size in each of the fractions when using the different solvent/ligand systems. With this said, it should also be noted that the original nanoparticle dispersions (prior to GXL fractionation) employed in all of these experiments contained particles of virtually identical size and size distribution. The *P*1 and *P*2 values for the control system of *n*-hexane/dodecanethiol were determined from the precipitation curve presented in Figure 3 using the method described above (and illustrated in Figure 2) where the absorbance value of 0.5 corresponded to a *P*1 value of 46.2 bar and the absorbance value of 0.4 corresponded to a *P*2 value of 46.5 bar. The *P*1 and *P*2 values for the other solvent–ligand combinations were determined similarly (corresponding the same absorbance values of 0.5 and 0.4, respectively) and are listed in Table 1. The pressure difference between two successive fractions is defined as ΔP where $\Delta P = P2 - P1$.

For the 2-methylpentane/dodecanethiol and the 3-methylpentane/dodecanethiol systems there is not a significant difference in the size distribution of the particles that constitute the first and second fractions which can be seen from the PDI values listed in Table 1. It is noted that these two systems yield nearly identical precipitation curves (Figure 6) stemming from the fact that they have only slightly different solvent structure. This similarity in solvent structure causes nanoparticles of comparable size and size distribution to destabilize and precipitate from solution at generally the same pressure conditions. However, the first fractions that were obtained from the methylpentane systems (i.e., 2-methylpentane/dodecanethiol and the 3-methylpentane/dodecanethiol) had were more monodisperse (PDI of 1.03) than the first fraction that was obtained from the *n*-hexane/dodecanethiol control system (PDI of 1.06). This difference in polydispersity can be attributed to the fact that the particles precipitate from solution over a wider pressure range (ΔP) in the case of the methylpentane solvents compared to the smaller pressure range over which precipitation occurs in the *n*-hexane system. The *n*-hexane solvent system results in a relatively steep precipitation curve (Figure 3) that requires that the nanoparticles be precipitated from solution over a smaller pressure gradient (ΔP), thereby affording less resolution in their size-selective separation.[39,44] CO_2-induced nanoparticle precipitation over a small pressure range is very sensitive to pressure

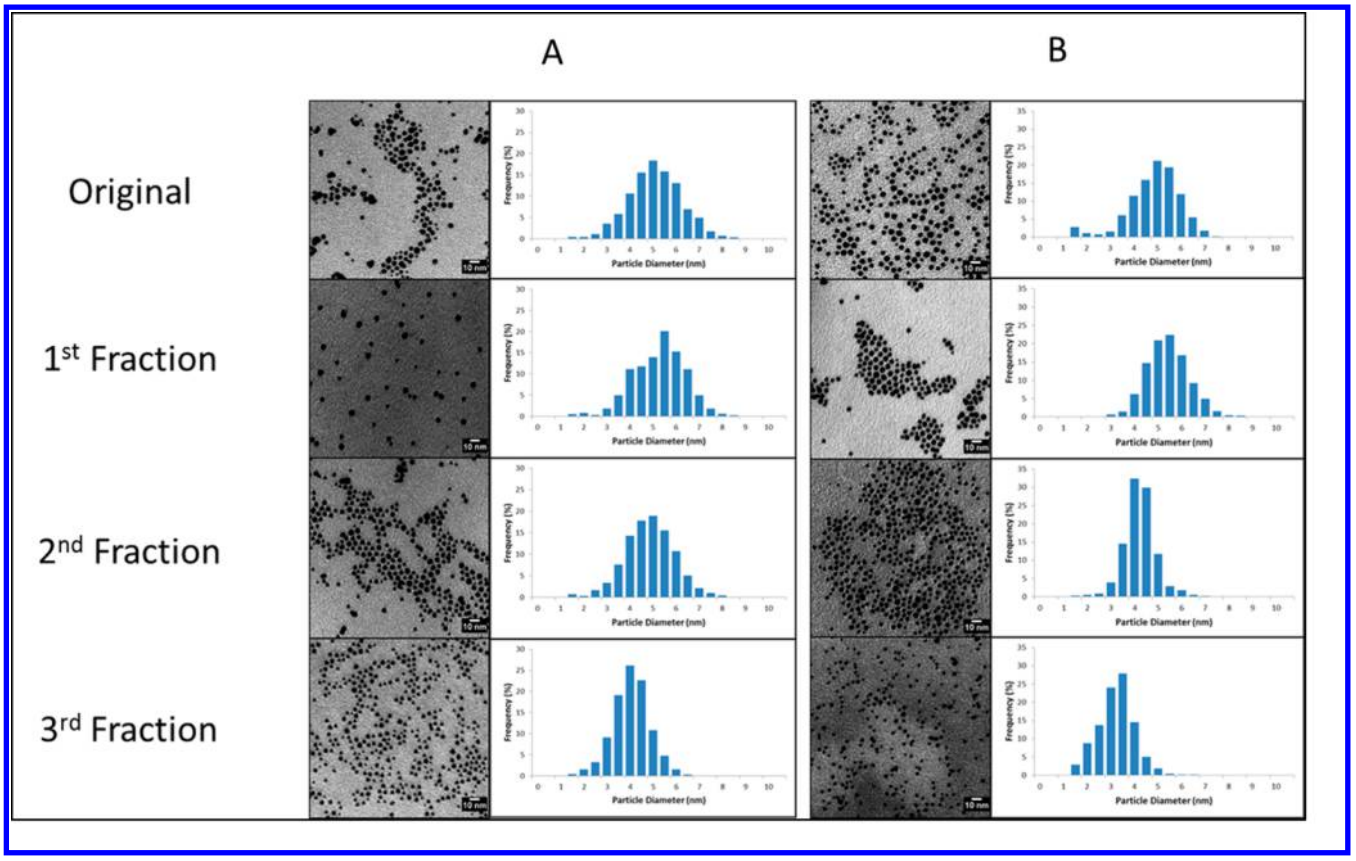

Figure 8. TEM micrographs and size distribution of dodecanethiol-stabilized gold nanoparticles dispersed in *n*-hexane (A) and 2,2-dimethylbutane (B) fractionated into three distinct size fractions using a CO_2 GXL. The pressures used for each of the fractions are listed in Table 1.

variations and other environmental conditions which can result in greater polydispersity of the particles precipitating from solution, as is illustrated in the results presented in Table 1.

Table 1 presents the experimental fractionation results for the 2,2-dimethylbutane/dodecanethiol and 2,3-dimethylbutane/dodecanethiol systems, where there are differences in the polydispersity values (i.e., PDI values) obtained from one system compared to the other. It is noted that the first fraction from both of the dimethylbutane systems (the 2,2-dimethylbutane/dodecanethiol and 2,3-dimethylbutane/dodecanethiol) has the same PDI value of 1.03. However, the second and third fractions obtained from the 2,2-dimethylbutane/dodecanethiol system exhibit lower PDI values than the respective fractions obtained from the 2,3-dimethylbutane/dodecanethiol system. This difference in polydispersity between these two systems can be attributed to the fact that the 2,2-dimethylbutane/dodecanethiol system has a lower P_i value and a less steep precipitation curve compared to the one for 2,3-dimethylbutane/dodecanethiol system. This results in the ability to have particles precipitate more gradually over a wider pressure range, thereby providing a slightly higher resolution to the fractionation process as a function of the applied CO_2 pressure. This, in turn, results in the ability to have particles of more uniform size precipitate from solution over a given pressure range, thereby resulting in lower PDI values for the 2,2-dimethylbutane/dodecanethiol system. Furthermore, Figure 8 presents a visual comparison of the results obtained from the 2,2-dimethylbutane/dodecanethiol system to those obtained for the control system of *n*-hexane/dodecanethiol, where each of the three fractions was collected at the conditions noted in Table 1. Because of the wider pressure range over which precipitation occurs in the 2,2-dimethylbutane/dodecanethiol system (i.e., less steep precipitation curve), this system yielded narrower size fractions when compared to the *n*-hexane/dodecanethiol system despite the fact that larger ΔP values were employed in collecting each of the three fractions. 2,2-Dimethylbutane provided the lowest P_i value among each of the solvents (*n*-hexane, 2-methylpentane, 3-methylpentane, 2,2-dimethylbutane, and 2,3-dimethylbutane) that were examined with this straight-chain ligand (i.e., dodecanethiol capped nanoparticles). Because of this, 2,2-dimethylbutane was used as a solvent in subsequent investigations into the effect that a branched ligand (*tert*-dodecanethiol) has on nanoparticle precipitation and fractionation in GXL systems.

2. Branched-Chain Ligand (*tert*-Dodecanethiol) and Various Solvents (*n*-Hexane and 2,2-Dimethylbutane). This set of experiments also involved varying the structure of the solvent employed while keeping the ligand structure consistent. However, a branched-chain stabilizing ligand (*tert*-dodecanethiol) was used instead of the straight-chain ligand (dodecanethiol) in examining the effect that the steric nature of the ligand has on gold nanoparticle precipitation. These experiments were performed using two different solvents. The first experiment involved using *tert*-dodecanethiol stabilized gold particles that were dispersed in 2,2-dimethylbutane solvent, and the second experiment involved using the same *tert*-dodecanethiol stabilized gold particles dispersed in *n*-hexane solvent (the control solvent). Recall that the 2,2-dimethylbutane was chosen as one of the solvents in this set of experiments because it provided the lowest P_i value among all of the solvents employed when investigating the straight-chain ligand systems.

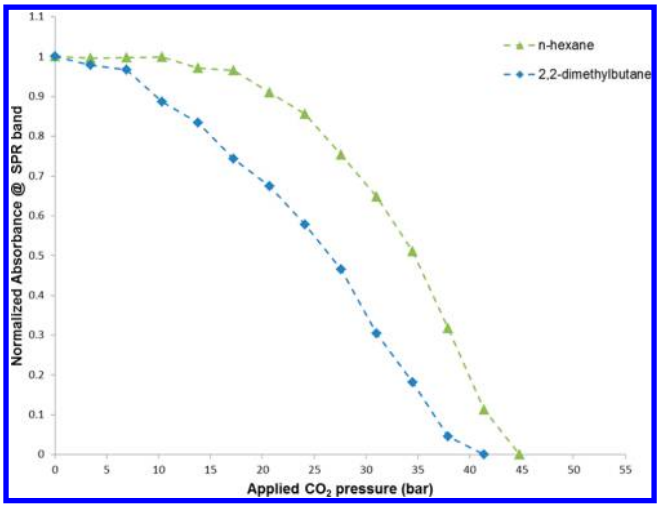

Figure 9. Precipitation curves for *tert*-dodecanethiol-coated gold nanoparticles dispersed in *n*-hexane and 2,2-dimethylbutane obtained by tracking the change in intensity of normalized SPR band using *in situ* UV−vis spectroscopy at different pressures.

2A. Effect of the Steric Nature of the Solvent on P_i Values with tert-Dodecanethiol as the Capping Ligand. Figure 9 presents the precipitation curves for the *n*-hexane/*tert*-dodecanethiol system and the 2,2-dimethylbutane/*tert*-dodecanethiol system, where it is clearly demonstrated that *tert*-dodecanethiol-capped particles precipitate at lower overall pressures in the 2,2-dimethylbutane solvent compared to the *n*-hexane solvent. The P_i for *n*-hexane/*tert*-dodecanethiol system is approximately 17 bar, and that for the 2,2-dimethylbutane/*tert*-dodecanethiol system is roughly 7 bar. It is noted that the normalized absorbance for the 2,2-dimethylbutane/*tert*-dodecanethiol system begins to fall slightly below 1.0 even at very low applied CO_2 pressures such that the P_i value may actually be lower than the approximated 7 bar listed here. In comparing the results in Figure 9 for the *tert*-dodecanethiol systems with the results in Figures 6 and 7 for the dodecanethiol system, it is observed that the branched-chain ligand gives significantly lower P_i values compared to its straight-chain counterpart in each of the solvents. The P_i values of ∼17 and ∼7 bar that were obtained from the *n*-hexane/*tert*-dodecanethiol and 2,2-dimethylbutane/*tert*-dodecanethiol systems, respectively, are radically different from the P_i values of ∼41 and ∼38 bar that were obtained from the *n*-hexane/dodecanethiol and 2,2-dimethylbutane/dodecanethiol systems, respectively.

The combination of a sterically hindered solvent (2,2-dimethylbutane) with a sterically hindered ligand (*tert*-dodecanethiol) results in further deterioration of the strength of the solvent−ligand interactions when compared to the use of the straight-chain solvent (*n*-hexane) and the straight-chain ligand (dodecanethiol) or even when compared to the use of the sterically hindered ligand (*tert*-dodecanethiol) with the straight-chain solvent. Obviously, the use of bulky, sterically hindered species in both capacities dramatically affects the ability of the GXL system to thermodynamically disperse nanoparticles, thereby drastically reducing the applied CO_2 pressure necessary for their removal from the CO_2 + solvent mixture. This reduction in the strength of the solvent−ligand

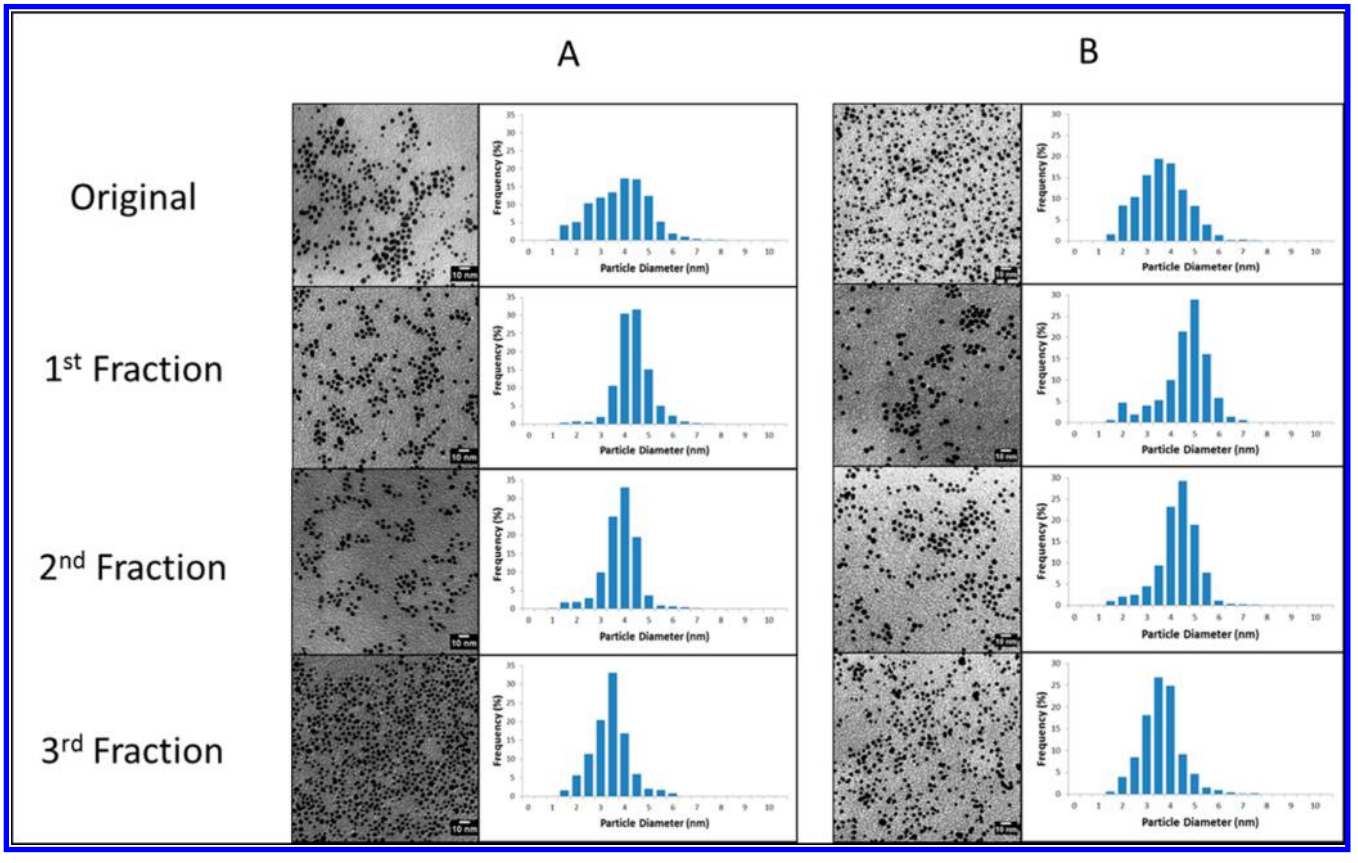

Figure 10. TEM micrographs and size distribution of *tert*-dodecanethiol-stabilized gold nanoparticles dispersed in *n*-hexane (A) and 2,2-dimethylbutane (B) fractionated into three distinct size fractions using a CO_2 GXL. The pressures used for each of the fractions are listed in Table 1.

interactions causes an almost 6-fold decrease in the P_i values for the 2,2-dimethylbutane/*tert*-dodecanethiol system (~7 bar) when compared to the *n*-hexane/dodecanethiol control system (~41 bar), stemming from a lower concentration of CO_2 being required to destabilize the nanoparticles from the solvent.

2B. Effect of the Steric Nature of the Solvent on GXL Fractionation Process with tert-Dodecanethiol-Capped Nanoparticles (Branched-Chain Ligand). Figure 10 and Table 1 present the results of the fractionation of *tert*-dodecanethiol-coated gold nanoparticles dispersed in *n*-hexane and 2,2-dimethylbutane, respectively. As stated earlier in this paper, the fractionation pressures (*P*1 and *P*2) that were employed in this set of experiments were determined from the precipitation curves for these systems (Figure 9), where *P*1 and *P*2 correspond to the normalized absorbance values of 0.5 and 0.4, respectively.

The data in Table 1 illustrate that successful GXL fractionations were achieved using the *n*-hexane/*tert*-dodecanethiol and 2,2-dimethylbutane/*tert*-dodecanethiol systems, where distinctly different size fractions were obtained coupled with PDI values that are very comparable to those obtained from the *n*-hexane/dodecanethiol control system. It is important to note that these successful fractionations were performed using much lower applied CO_2 pressures, and higher ΔP values, than those necessary in the *n*-hexane/dodecanethiol control system. Simply on the basis of the desire to lower the overall operating pressure in a fractionation process of this type, one might consider the combination of the 2,2-dimethylbutane solvent and the *tert*-dodecanethiol ligand capped nanoparticles to be the optimal system among those that were investigated in this study.

One important parameter that has not been discussed to this point, but is important from a process control point-of-view, is the time necessary to conduct each stage of the GXL fractionation process. In the systems where dodecanethiol was used as the stabilizing ligand of choice, approximately 20–30 min was required to carry out each successive fractionation step, and the entire GXL fractionation process was completed in about an hour. However, for the systems in which particles were coated with *tert*-dodecanethiol, each fractionation step took around 90–120 min and the entire process took more than 4 h.

This increase in processing time results from the fact that the *tert*-dodecanethiol ligand coated gold nanoparticles precipitate from solution at lower overall applied CO_2 pressures, and as such, they precipitate more slowly because of the different thermophysical properties of the solvent mixture at those conditions. These GXL systems have higher viscosities and lower diffusion coefficients at the lower applied CO_2 pressures (i.e., lower CO_2 concentration) than they do when subjected higher CO_2 pressures.[64] As a result, there is an inherent trade-off between processing time and the pressures required to precipitate particles from solution in these different solvent/ligand systems, and it may not be possible to eliminate this issue completely without major process modifications.[44] This will be an important factor to consider when scaling up the process and in determining optimum operating conditions.

CONCLUSION

In summary, through the simple adjustment in the solvent–ligand interactions by manipulating the steric nature of the solvent and ligand, we were able to reduce the applied pressure for gold-nanoparticle precipitation from GXLs. From the various combination of solvents/ligands employed in this study to understand the influence of the steric nature of solvents/ligands on nanoparticle precipitation and fractionation, it was deduced that the 2,2-dimethylbutane/*tert*-dodecanethiol system offered the largest reduction in P_i value while retaining good fractionation characteristics. This almost 6-fold reduction in P_i value from 41.4 bar (*n*-hexane/dodecanethiol system) to 6.9 bar (2,2-dimethylbutane/*tert*-dodecanethiol) can be attributed to the reduction in solvent–ligand interactions due to the steric hindrance offered by the branched ligand and branched solvent. By employing both a branched ligand and a branched solvent, successful fractionations were obtained at lower overall pressures and higher ΔP values compared to the straight-chain ligand and straight-chain solvent control system. This suggests that one can influence the process parameters critical to the GXL size-selective fractionation process by simply changing the physical interactions between the nanoparticles and the solvent, and this strategy can be used to effectively tune these parameters.

ASSOCIATED CONTENT

Supporting Information

Supplementary figures pertaining to experimental volumetric expansion data. This material is available free of charge via the Internet at http://pubs.acs.org.

AUTHOR INFORMATION

Corresponding Author

*E-mail croberts@eng.auburn.edu; Ph 334-844-2303 (C.B.R.).

Notes

The authors declare no competing financial interest.

ACKNOWLEDGMENTS

This research was made possible in part from a grant from the BP/The Gulf of Mexico Research Initiative through the Consortium for Molecular Engineering of Dispersant Systems. The authors also thank Dr. Michael Miller and the Auburn University Research and Instrumentation Facility for access to the transmission electron microscope. The authors also greatly appreciate technical discussions and assistance from Dr. Steven R. Saunders at Georgia Institute of Technology and Jennifer N. Duggan at Auburn University.

REFERENCES

(1) Pankhurst, Q. A.; Connolly, J.; Jones, S. K.; Dobson, J. Applications of magnetic nanoparticles in biomedicine. *J. Phys. D: Appl. Phys.* **2003**, *36*, R167.

(2) Tartaj, P.; Morales, M. D. P.; Veintemillas-Verdaguer, S.; Gonzalez-Carreno, T.; Serna, C. J. The preparation of magnetic nanoparticles for applications in biomedicine. *J. Phys. D: Appl. Phys.* **2003**, *36*, R182–R197.

(3) Karimi, Z.; Karimi, L.; Shokrollahi, H. Nano-magnetic particles used in biomedicine: Core and coating materials. *Mater. Sci. Eng., C* **2013**, *33*, 2465–75.

(4) Lim, J.; Majetich, S. a. Composite magnetic–plasmonic nanoparticles for biomedicine: Manipulation and imaging. *Nano Today* **2013**, *8*, 98–113.

(5) Hurst, K. M.; Roberts, C. B.; Ashurst, W. R. Characterization of gas-expanded liquid-deposited gold nanoparticle films on substrates of varying surface energy. *Langmuir* **2011**, *27*, 651–5.

(6) Berry, K. R.; Russell, A. G.; Blake, P. a.; Keith Roper, D. Gold nanoparticles reduced in situ and dispersed in polymer thin films: optical and thermal properties. *Nanotechnology* **2012**, *23*, 375703.

(7) Haruta, M.; Daté, M. Advances in the catalysis of Au nanoparticles. *Appl. Catal., A* **2001**, *222*, 427−437.
(8) Daniel, M.-C.; Astruc, D. Gold nanoparticles: assembly, supramolecular chemistry, quantum-size-related properties, and applications toward biology, catalysis, and nanotechnology. *Chem. Rev.* **2004**, *104*, 293−346.
(9) Hervés, P.; Pérez-Lorenzo, M.; Liz-Marzán, L. M.; Dzubiella, J.; Lu, Y.; Ballauff, M. Catalysis by metallic nanoparticles in aqueous solution: model reactions. *Chem. Soc. Rev.* **2012**, *41*, 5577−87.
(10) Mikami, Y.; Dhakshinamoorthy, A.; Alvaro, M.; García, H. Catalytic activity of unsupported gold nanoparticles. *Catal. Sci. Technol.* **2013**, *3*, 58.
(11) Mahajan, D.; Gütlich, P.; Ensling, J. Evaluation of nanosized iron in slurry-phase Fischer−Tropsch synthesis. *Energy Fuels* **2003**, *17*, 1210−1221.
(12) Kelsen, V.; Wendt, B.; Werkmeister, S.; Junge, K.; Beller, M.; Chaudret, B. The use of ultrasmall iron(0) nanoparticles as catalysts for the selective hydrogenation of unsaturated C-C bonds. *Chem. Commun. (Cambridge, U. K.)* **2013**, *49*, 3416−8.
(13) Teja, A. S.; Koh, P.-Y. Synthesis, properties, and applications of magnetic iron oxide nanoparticles. *Prog. Cryst. Growth Charact. Mater.* **2009**, *55*, 22−45.
(14) Andreas, K.; Georgieva, R.; Ladwig, M.; Mueller, S.; Notter, M.; Sittinger, M.; Ringe, J. Highly efficient magnetic stem cell labeling with citrate-coated superparamagnetic iron oxide nanoparticles for MRI tracking. *Biomaterials* **2012**, *33*, 4515−25.
(15) Lee, N.; Hyeon, T. Designed synthesis of uniformly sized iron oxide nanoparticles for efficient magnetic resonance imaging contrast agents. *Chem. Soc. Rev.* **2012**, *41*, 2575−89.
(16) Poole Jr., C. P.; Owens, F. *Introduction to Nanotechnology*; Wiley- Interscience: Hoboken, NJ, 2003.
(17) El-Sayed, M. A. Small is different: shape-, size-, and composition-dependent properties of some colloidal semiconductor nanocrystals. *Acc. Chem. Res.* **2004**, *37*, 326−33.
(18) Sun, S.; Zeng, H. Size-controlled synthesis of magnetite nanoparticles. *J. Am. Chem. Soc.* **2002**, *124*, 8204−8205.
(19) Sun, S. Monodisperse FePt nanoparticles and ferromagnetic FePt nanocrystal superlattices. *Science* **2000**, *287*, 1989−1992.
(20) Sun, Y.; Xia, Y. Shape-controlled synthesis of gold and silver nanoparticles. *Science* **2002**, *298*, 2176−9.
(21) Deng, H.; Li, X.; Peng, Q.; Wang, X.; Chen, J.; Li, Y. Monodisperse magnetic single-crystal ferrite microspheres. *Angew. Chem.* **2005**, *117*, 2842−2845.
(22) Xiong, J.; Wu, X.; Xue, Q. One-step route for the synthesis of monodisperse aliphatic amine-stabilized silver nanoparticles. *Colloids Surf., A* **2013**, *423*, 89−97.
(23) Li, Y.; Liu, S.; Yao, T.; Sun, Z.; Jiang, Z.; Huang, Y.; Cheng, H.; Huang, Y.; Jiang, Y.; Xie, Z.; Pan, G.; Yan, W.; Wei, S. Controllable synthesis of gold nanoparticles with ultrasmall size and high monodispersity via continuous supplement of precursor. *Dalton Trans.* **2012**, *41*, 11725−30.
(24) Liu, X.; Xu, H.; Xia, H.; Wang, D. Rapid seeded growth of monodisperse, quasi-spherical, citrate-stabilized gold nanoparticles via H_2O_2 reduction. *Langmuir* **2012**, *28*, 13720−6.
(25) Yavuz, C. T.; Mayo, J. T.; Yu, W. W.; Prakash, A.; Falkner, J. C.; Yean, S.; Cong, L.; Shipley, H. J.; Kan, A.; Tomson, M.; Natelson, D.; Colvin, V. L. Low-field magnetic separation of monodisperse Fe_3O_4 nanocrystals. *Sciences (N. Y.)* **2006**, *314*, 964−7.
(26) Tasci, T. O.; Manangon, E.; Fernandez, D. P.; Johnson, W. P.; Gale, B. K. Separation of magnetic nanoparticles by cyclical electrical field flow fractionation. *IEEE Trans. Magn.* **2013**, *49*, 331−335.
(27) Siebrands, T.; Giersig, M.; Mulvaney, P.; Fischer, C. H. Steric exclusion chromatography of nanometer-sized gold particles. *Langmuir* **1993**, *9*, 2297−2300.
(28) Wei, G. T.; Liu, F. K.; Wang, C. R. Shape separation of nanometer gold particles by size-exclusion chromatography. *Anal. Chem.* **1999**, *71*, 2085−91.
(29) Novak, J. P.; Nickerson, C.; Franzen, S.; Feldheim, D. L. Purification of molecularly bridged metal nanoparticle arrays by centrifugation and size exclusion chromatography. *Anal. Chem.* **2001**, *73*, 5758−5761.
(30) Siswoyo; Lim, L. W.; Takeuchi, T. Separation of gold nanoparticles with a monolithic silica capillary column in liquid chromatography. *Anal. Sci.* **2012**, *28*, 107−13.
(31) Sakai-Kato, K.; Ota, S.; Takeuchi, T.; Kawanishi, T. Size separation of colloidally dispersed nanoparticles using a monolithic capillary column. *J. Chromatogr., A* **2011**, *1218*, 5520−6.
(32) Akbulut, O.; Mace, C. R.; Martinez, R. V.; Kumar, A. a; Nie, Z.; Patton, M. R.; Whitesides, G. M. Separation of nanoparticles in aqueous multiphase systems through centrifugation. *Nano Lett.* **2012**, *12*, 4060−4.
(33) Surugau, N.; Urban, P. L. Electrophoretic methods for separation of nanoparticles. *J. Sep. Sci.* **2009**, *32*, 1889−906.
(34) Ho, S.; Critchley, K.; Lilly, G. D.; Shim, B.; Kotov, N. a. Free flow electrophoresis for the separation of CdTe nanoparticles. *J. Mater. Chem.* **2009**, *19*, 1390.
(35) Liang, H.-W.; Wang, L.; Chen, P.-Y.; Lin, H.-T.; Chen, L.-F.; He, D.; Yu, S.-H. Carbonaceous nanofiber membranes for selective filtration and separation of nanoparticles. *Adv. Mater.* **2010**, *22*, 4691−5.
(36) Trefry, J. C.; Monahan, J. L.; Weaver, K. M.; Meyerhoefer, A. J.; Markopolous, M. M.; Arnold, Z. S.; Wooley, D. P.; Pavel, I. E. Size selection and concentration of silver nanoparticles by tangential flow ultrafiltration for SERS-based biosensors. *J. Am. Chem. Soc.* **2010**, *132*, 10970−2.
(37) Fletcher, D. Fine particle high gradient magnetic entrapment. *IEEE Trans. Magn.* **1991**, *27*, 3655−3677.
(38) Bishop, K. J. M.; Wilmer, C. E.; Soh, S.; Grzybowski, B. a Nanoscale forces and their uses in self-assembly. *Small* **2009**, *5*, 1600−30.
(39) Saunders, S. R.; Roberts, C. B. Size-selective fractionation of nanoparticles at an application scale using CO_2 gas-expanded liquids. *Nanotechnology* **2009**, *20*, 475605.
(40) Anand, M.; Odom, L. A.; Roberts, C. B. Finely controlled size-selective precipitation and separation of CdSe/ZnS semiconductor nanocrystals using CO_2-gas-expanded liquids. *Langmuir* **2007**, *23*, 7338−43.
(41) McLeod, M. C.; Anand, M.; Kitchens, C. L.; Roberts, C. B. Precise and rapid size selection and targeted deposition of nanoparticle populations using CO_2 gas expanded liquids. *Nano Lett.* **2005**, *5*, 461−5.
(42) Jessop, P. G.; Subramaniam, B. Gas-expanded liquids. *Chem. Rev.* **2007**, *107*, 2666−94.
(43) McLeod, M. C.; Kitchens, C. L.; Roberts, C. B. CO_2-expanded liquid deposition of ligand-stabilized nanoparticles as uniform, wide-area nanoparticle films. *Langmuir* **2005**, *21*, 2414−8.
(44) Saunders, S. R.; Roberts, C. B. Tuning the precipitation and fractionation of nanoparticles in gas-expanded liquid mixtures. *J. Phys. Chem. C* **2011**, *115*, 9984−9992.
(45) Saunders, S. R.; Roberts, C. B. Nanoparticle separation and deposition processing using gas expanded liquid technology. *Curr. Opin. Chem. Eng.* **2012**, *1*, 1−11.
(46) Anand, M.; McLeod, M. C.; Bell, P. W.; Roberts, C. B. Tunable solvation effects on the size-selective fractionation of metal nanoparticles in CO_2 gas-expanded solvents. *J. Phys. Chem. B* **2005**, *109*, 22852−9.
(47) Brust, M.; Walker, M.; Bethell, D.; Schiffrin, D. J.; Whyman, R. Synthesis of thiol-derivatised gold nanoparticles in a two-phase liquid system. *J. Chem. Soc., Chem. Commun.* **1994**, 801.
(48) Goulet, P. J. G.; Lennox, R. B. New insights into Brust-Schiffrin metal nanoparticle synthesis. *J. Am. Chem. Soc.* **2010**, *132*, 9582−4.
(49) Sigman, M. B.; Saunders, A. E.; Korgel, B. A. Metal nanocrystal superlattice nucleation and growth. *Langmuir* **2004**, *20*, 978−983.
(50) Amendola, V.; Meneghetti, M. Size evaluation of gold nanoparticles by UV−vis spectroscopy. *J. Phys. Chem. C* **2009**, *113*, 4277−4285.

(51) Haiss, W.; Thanh, N. T. K.; Aveyard, J.; Fernig, D. G. Determination of size and concentration of gold nanoparticles from UV-vis spectra. *Anal. Chem.* **2007**, *79*, 4215−21.
(52) Alvarez, M. M.; Khoury, J. T.; Schaaff, T. G.; Shafigullin, M. N.; Vezmar, I.; Whetten, R. L. Optical absorption spectra of nanocrystal gold molecules. *J. Phys. Chem. B* **1997**, *101*, 3706−3712.
(53) Creighton, J. A.; Eadon, D. G. Ultraviolet-visible absorption spectra of the colloidal metallic elements. *J. Chem. Soc., Faraday Trans.* **1991**, *87*, 3881.
(54) Mutelet, F.; Vitu, S.; Privat, R.; Jaubert, J.-N. Solubility of CO_2 in branched alkanes in order to extend the PPR78 model (predictive 1978, Peng−Robinson EOS with temperature-dependent k_{ij} calculated through a group contribution method) to such systems. *Fluid Phase Equilib.* **2005**, *238*, 157−168.
(55) Anand, M.; You, S.-S.; Hurst, K. M.; Saunders, S. R.; Kitchens, C. L.; Ashurst, W. R.; Roberts, C. B. Thermodynamic analysis of nanoparticle size selective fractionation using gas-expanded liquids. *Ind. Eng. Chem. Res.* **2008**, *47*, 553−559.
(56) Fuente, J. C. De; Peters, C. J.; Arons, J. D. S. Volume expansion in relation to the gas−antisolvent process. *Science* **2000**, *17*, 13−23.
(57) Martin, J. E.; Wilcoxon, J. P.; Odinek, J.; Provencio, P. Control of the interparticle spacing in gold nanoparticle superlattices. *J. Phys. Chem. B* **2000**, *104*, 9475−9486.
(58) Fowkes, F. Surface effects of anisotropic London dispersion forces in n-alkanes. *J. Phys. Chem.* **1980**, *84*, 510−512.
(59) Tancrède, P.; Patterson, D.; Bothorel, P. Interactions in alkane systems by depolarized Rayleigh scattering and calorimetry. Part 2. Orientational order in systems containing hexadecane isomers of different. *J. Chem. Soc., Faraday Trans.* **1977**, *2*, 29−39.
(60) Brown, W. H.; Foote, C. S.; Iverson, B. L.; Anslyn, E. V.; Novak, B. M. *Organic Chemistry*; Cengage Learning: Independence, KY, 2011.
(61) Paulini, R.; Frankamp, B.; Rotello, V. Effects of branched ligands on the structure and stability of monolayers on gold nanoparticles. *Langmuir* **2002**, 2368−2373.
(62) Kelter, P.; Michael, M.; Scott, A. *Chemistry: The Practical Science*; Cengage Learning: Independence, KY, 2008; Vol. *10*.
(63) Murray, C.; Norris, D.; Bawendi, M. Synthesis and characterization of nearly monodisperse CdE (E = sulfur, selenium, tellurium) semiconductor nanocrystallites. *J. Am. Chem. Soc.* **1993**, 8706−8715.
(64) Scurto, A. M.; Hutchenson, K.; Subramaniam, B. Gas-expanded liquids: fundamentals and applications. *Symposium A Quarterly Journal In Modern Foreign Literatures* **2009**, 3−37.